JACS
JOURNAL OF THE AMERICAN CHEMICAL SOCIETY
Article
pubs.acs.org/JACS

Step Flow Versus Mosaic Film Growth in Hexagonal Boron Nitride

Jiong Lu,[†,‡] Pei Shan Emmeline Yeo,[†,∥] Yi Zheng,[†] Hai Xu,[†,‡] Chee Kwan Gan,[∥] Michael B. Sullivan,[∥] A.H. Castro Neto,[‡,§] and Kian Ping Loh*[,†,‡]

[†]Department of Chemistry, National University of Singapore, 3 Science Drive 3, Singapore 117543
[‡]Graphene Research Centre, National University of Singapore, 6 Science Drive 2, Singapore 117546
[§]Department of Physics, National University of Singapore, 2 Science Drive 3, Singapore 117542
[∥]Institute of High Performance Computing, 1 Fusionopolis Way, #16-16 Connexis, Singapore 138632

Supporting Information

ABSTRACT: Many emerging applications of hexagonal boron nitride (h-BN) in graphene-based nanoelectronics require high-quality monolayers as the ultrathin dielectric. Here, the nucleation and growth of h-BN monolayer on Ru(0001) surface are investigated using scanning tunneling microscopy with a view toward understanding the process of defect formation on a strongly interacted interface. In contrast to homoelemental bonding in graphene, the heteroelemental nature of h-BN gives rise to growth fronts with elemental polarity. This can have consequences in the different stages of film growth, from the nucleation of h-BN magic clusters and their sintering to form compact triangular islands to the growth of patchwork mosaic monolayer with a high density of misfit boundaries. The parallel alignment of triangular islands on the same terrace produces translational fault lines when growth fronts merge, while antiparallel alignment of islands on adjacent terraces produces non-bonded fault lines between domains terminated by like atoms. With these insights into the generation of void defects and fault lines at grain boundaries, we demonstrate a strategy to obtain high-quality h-BN monolayer film based on step flow growth.

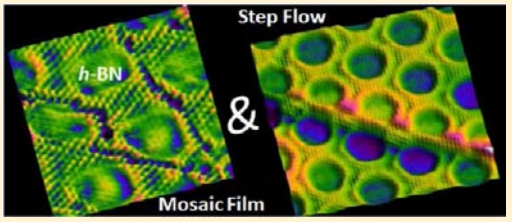

INTRODUCTION

Hexagonal boron nitride (h-BN), the two-dimensional isoelectronic compound of graphene, has recently received considerable attention owing to its successful incorporation in graphene-based hybrid nanodevices.[1−4] Analogous to graphene, diatomic B−N pairs in single-layer h-BN are packed in a honeycomb structure with sp^2-hybridized covalent bonding, but it is differentiated by the ionicity of its bonds. The bulk h-BN compound has excellent mechanical and thermal properties and high chemical stability.[5,6] In contrast to semimetallic graphene, h-BN is a wide direct band gap insulator, which makes it a promising electrically insulating substrate for graphene electronics.[1,7] Indeed, stacking graphene on h-BN flake exfoliated from high-pressure high-temperature (HPHT) grown crystals yields the highest mobility ever reported for any substrate because of the atomic flatness of h-BN and absence of charge traps on h-BN surface.[1,7]

For technological applications, it is crucial to minimize structural defects and synthesize high quality h-BN films on a large scale. To this end, chemical vapor deposition (CVD) using BN precursors like borazine ($N_3B_3H_6$)[8,9] and ammonia borane (NH_3−BH_3) is a promising approach for large-scale growth of h-BN.[6] However, films produced by CVD have a higher density of defects and are not comparable to flakes exfoliated from HPHT crystal. The nature of defects in h-BN is not well understood; dislocation may arise from either topological defects or homoelemental bonding. For example, topological defects due to nonhexagon rings are common in graphene, and depending on the symmetry of the structure, local Gaussian curvature can be induced in the sheet. Understanding the nature of defects is crucial because they determine the material properties at the macroscopic scale.[10] Depending on synthesis conditions, non-equilibrium defects can be produced that cannot be annealed once they are formed due to its high formation energy. Fault lines in the material allow impurities to diffuse or foreign atoms to be intercalated. Finally, defects, if engineered in a controllable manner, can also offer great flexibility in manipulating the electronic, magnetic, and mechanical properties of two-dimensional materials.[11−13]

The growth of single-layer h-BN by CVD has been extensively studied on various transition metals like Ni(111),[14−17] Cu(111),[18] Ir(111),[19] Pt(111),[20−22] Rh(111),[8,9,23−25] Ru(0001),[26,27] and etc. A wide polytype of h-BN superstructures had been previously grown on metal surface, depending on the lattice matching condition and the interaction strength between h-BN and underlying metal. The strength of interfacial bonding is determined by the amount of charge transfer between h-BN π states and metal d band, which decreases if the d-shell of metal atoms is full. Hence, Cu(d^{10}) or Pt(d^9) with a greater filled d-shell yields a weaker bonding to h-BN compared to Ru(d^7). Moreover, a commensurate layer of h-BN can only be grown on substrate with close lattice matching to h-BN. For Ru and Rh surfaces with a large lattice mismatch

Received: December 3, 2012
Published: January 17, 2013

 © 2013 American Chemical Society dx.doi.org/10.1021/ja3117735 | J. Am. Chem. Soc. 2013, 135, 2368−2373

and strong bonding with h-BN, the resulting h-BN topology becomes highly corrugated (~1.5 Å) and periodic "nanomesh" structures with moiré pores (lower parts) and wires (elevated parts) are formed.[20] The moiré periodicity is determined by the lattice matching condition: $n_{BN} \times a_{BN} = n_M \times a_M$, where n_{BN} (n_M) is the number of unit cell repetitions of h-BN (metal), while a_{BN} (a_M) is the corresponding lattice constant.[28] Therefore, h-BN nanomesh unit cells coincide with a 12 × 12 unit cell for Ru and Pt and 9 × 9 for Pt. The relationship between the moiré periodicity and the defect formation during growth remains largely unexplored. There is also a lack of atomistic insight on the formation of vacancies and grain boundaries and the non-equilibrium conditions associated with it. To this end, we carried out a systematic STM study of the nucleation of h-BN on the Ru(0001) surface with a view toward understanding the formation of non-equilibrium defects and how these can be suppressed. We discover that the presence of elemental polarity in h-BN gives rise to special alignment of growth clusters not seen in graphene and that the interactions with the metal substrate have fundamental effects on the defect growth. This poses potentially greater challenge to synthesize defect-free h-BN film by CVD on certain substrates.

EXPERIMENTAL SECTION

Sample Preparation. The experiments were performed in an ultrahigh-vacuum chamber with a base pressure of 2×10^{-10} mbar. The Ru(0001) surface was carefully cleaned using repeated cycles of argon ion sputtering at room temperature $p(Ar) = 2 \times 10^{-5}$ mbar, 1.0 keV, followed by annealing in an O_2 partial pressure of 2×10^{-7} mbar at 1000 K, then flashing annealing to 1600 K. Single-layer h-BN islands were grown on the Ru(0001) by thermal decomposition of vaporized borazine at a partial pressure of 5×10^{-8} mbar. After growth, the sample was transferred into the main chamber and characterized by a SPECS STM 150 Aarhus unit with the Nanonis (SPECS) SPM control system.

Simulation Methods. We performed the density functional theory (DFT) calculations using the SIESTA package.[29] The electronic relaxation was terminated when the energy difference is <0.1 meV. The local density approximation was used for the exchange–correlation functional. Troullier–Martins pseudopotentials were used to describe the interactions due to ions and core electrons.[30] The mesh cutoff is 250 Ry. We used double-ζ with polarization (DZP) atomic basis functions for B, N, and bulk Ru atoms, while Ru atoms at the surface had additional f polarization orbitals. We added 5s DZP "floating orbitals" above the Ru surface to better describe the decay of the wave functions into the vacuum at the surface, which results in a better match between the experimental and calculated surface energies[31] (see Supporting Information (SI) for details).

RESULTS AND DISCUSSION

Magic Clusters during Initial Growth. To observe the initial stages of nucleation of h-BN islands, we exposed a clean Ru(0001) surface to a low dosage of borazine [9.6 Langmuir (L)] with the substrate heated to 700 K. STM images show that Ru surface becomes uniformly decorated with triangular h-BN clusters, as shown in Figure 1a,b. Our DFT calculation shows the N-terminated edge in h-BN islands adsorbed on Ru is energetically more favorable compared to B-terminated edge. The formation energy of N-terminated three-ring h-BN cluster on Ru is lower in energy than the B-terminated one by 1.87 eV (Figure S1). The consequence of this is a symmetry reduction of the h-BN islands such that they manifest almost entirely as triangular clusters, in contrast to the growth of high-symmetry hexagonal graphene islands in the initial stages of CVD.[32−35]

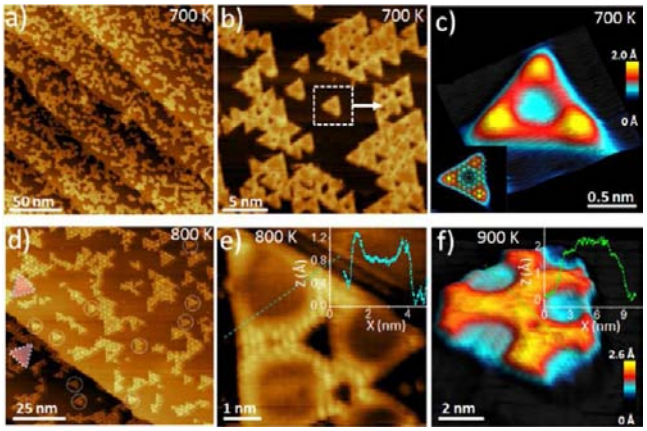

Figure 1. STM images of the initial stages of nucleation of h-BN clusters at different temperatures. (a) The Ru(0001) surface is imaged directly after exposure to 9.6 L borazine gas at 700 K. (b) Homogeneously sized h-BN "magic clusters" (1.5 nm). (c) 3D STM image of triangular BN clusters with the proposed structure in the inset of (c). (d) Same exposure to borazine but heated to 800 K (4×10^{-8} mbar, 4 min). (e) Magnified view of 5 nm sized triangular BN islands circled in (d). Inset: height profile recorded along the line in (e) shows the edge of triangle islands is 0.4 Å higher than that of the center, which indicates the edge of h-BN islands are terminated with hydrogen. (f) Sample (d) was heated at 900 K to remove edge hydrogen atoms and height profiles show that the center of island is now higher than edge. Characteristic moiré superstructures are due to the coupling of h-BN with Ru substrate.

Figure 1b shows the magnified STM image of homogeneously sized magic clusters with lateral size of 1.5 nm, which act as the basic building block for the bigger clusters (4 nm base width) shown in Figure 1d,e. One triangular h-BN cluster at the initial stage of growth is highlighted in Figure 1c. Its center region appears darker compared to the corner areas due to its stronger interaction with the substrate, which gives rise to a "bowl-like" adsorption configuration. It is highly likely that the edge atoms are passivated with hydrogen (inset of Figure 1c). The presence of hydrogen atoms in the initial stage of growth of h-BN has also been proposed in a previous report.[23] A recent study of h-BN grown on Ir(111) also revealed that dehydrogenation of borazine is observed at temperatures higher than 250 K and complete desorption of hydrogen species extends up to 900 K.[19]

Figure 1d displays the growth of larger-sized clusters after exposing Ru to 9.6 L borazine gas at 800 K. The majority of the islands observed here are ~4 nm in size (circled in Figure 1d). These clusters are formed by the coalescence of three 1.5 nm bowl-like h-BN clusters which inadvertently trap a triangular void in the center region, as magnified in Figure 1e. The height profile in the inset of Figure 1e clearly reveals that the edge of bowl is 0.4 Å higher than the center region of the bowl. This topographic structure is reminiscent of the moiré "pore" and "wire" structure imaged in h-BN nanomesh on Ru(0001). Upon heating to 900 K, the topographic contrast of h-BN clusters is reversed, and the center region becomes brighter than the edge (Figure 1f), and the center region is now 0.5 Å higher than the edge (inset of Figure 1f) from height profile analysis. This can be rationalized by the desorption of the edge hydrogen atoms at high temperature, thus allowing the edge atoms to couple to the Ru substrate. At a heating temperature of 900 K, the triangle voids in h-BN were repaired due to a move toward thermal equilibrium. These suggest that small h-

dx.doi.org/10.1021/ja3117735 | J. Am. Chem. Soc. 2013, 135, 2368−2373

BN islands are able to reconstruct around well-defined geometrical voids at elevated temperature.

Shape and Alignment of Larger Domain. The formation of compact islands without voids is one of the prerequisites for growing high-quality films. Compact h-BN islands exhibiting well-defined moiré "nanomesh" structures can be synthesized at temperatures >950 K. STM images in Figure 2a show the growth of compact h-BN islands with lateral sizes

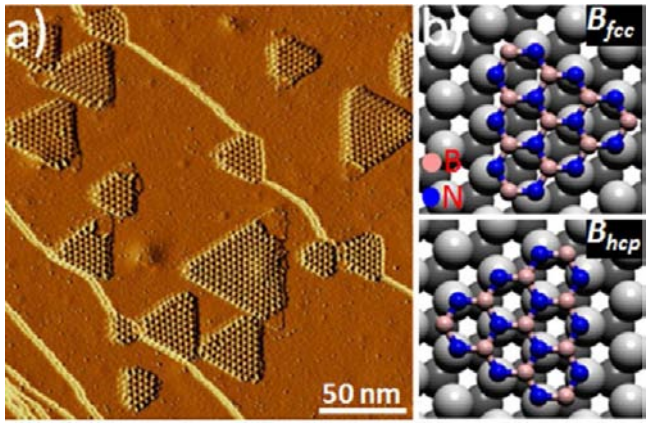

Figure 2. (a) Derivative STM image of antiparallel triangular h-BN islands grown on adjacent terraces after exposoure 5 L borazine at 950 K. (b) Scheme shows the $N_{top}B_{fcc}$ and $N_{top}B_{hcp}$ adsorption configurations. Light- and dark-gray balls represent Ru atoms in the top and second layers, respectively.

ranging from 10 to 50 nm after exposure of Ru to 5 L borazine gas at 950 K. Most of the h-BN islands are triangular, while the rest show truncated triangular shape (with three long and three short edges). Intriguingly, the orientations of these triangular islands are rotated 60° between adjacent steps (Figures 2a and S2), giving rise to antiparallel domains which alternate across the steps. To explain the alternating geometry of these islands between adjacent steps, we have to look at the atomistic model of the adsorption of h-BN islands on the hexagonal closed packed (hcp) Ru(0001) surface. Due to the fact that h-BN has elemental polarity, special atom−substrate interaction can dictate the orientation of the triangular islands. Depending on the local bonding environment of the Ru atoms with N and B atoms, the unit cells of h-BN can be divided into regions with different coordination with the metal substrate. As shown in the schematic of Figure 2b, the notation of $N_{top}B_{hcp}$ and $N_{top}B_{fcc}$ refer to the regions where B atoms sit in hcp hollow sites or face centered cubic (fcc) hollow sites, respectively, with N atoms sitting directly on top of Ru atoms. For infinite *h*-BN on transition metals, the N atoms preferentially sit directly on top on a Ru atom due to the strong hybridization of the N lone pair with Ru *d* states. To compare the energy difference between h-BN clusters in the $N_{top}B_{fcc}$ or $N_{top}B_{hcp}$ configurations on Ru(0001), we investigate the adsorption energies of one-, three-, and six-ring h-BN clusters on Ru(0001) hexagonal supercells with lateral size of 10.66, 13.33, and 15.99 Å, respectively. Our DFT results show that $N_{top}B_{fcc}$ is the most stable binding configuration and the energy difference between $N_{top}B_{fcc}$ (fcc domain) and $N_{top}B_{hcp}$ (hcp domain) is ∼40 meV/B atom, independent of the cluster size (see SI for details). In order to adopt the energetically favorable $N_{top}B_{fcc}$ absorption configuration exclusively, all the triangular islands become aligned in the same direction on one terrace. However, it is necessary for the h-BN triangles to rotate 60° consecutively between adjacent terraces to accommodate the alternating ABAB packing of the hcp Ru stepped surface, thus giving rise to the antiparallel arrangement of the h-BN islands observed in Figure 2. On Cu or Ni substrate, the most stable binding configuration adopted by the h-BN islands is also the fcc ($N_{top}B_{fcc}$) type. However, all the fcc domains are parallel-aligned on the same or adjacent terraces due to the fcc packed crystal structure. In addition, the energy difference between hcp and fcc domains is significantly reduced due to the weak interfacial bonding (∼9.2 meV/B atom for Ni), this will result in a higher percentage of hcp domain on Ni(111) or Cu(111) surfaces, compared to that on Ru(0001).

Void Defects and Fault Lines. Figure 3a−c documents the merging of the islands and the generation of voids when the

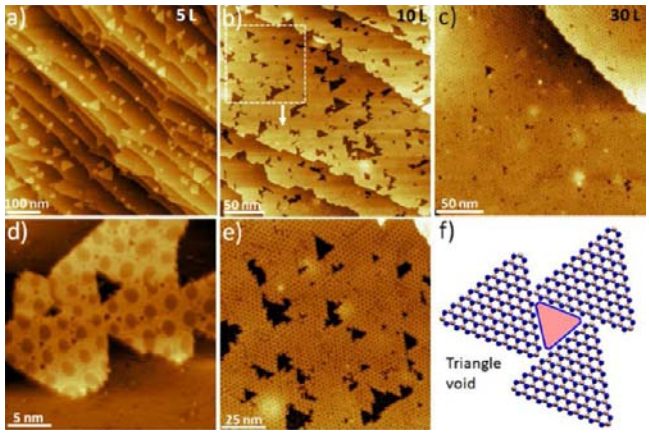

Figure 3. STM images of Ru(0001) surface after exposure to different amounts of borazine (a), 5 L (b) 10 L, (c) 30 L at 950 K. (d) The coalescence of triangular islands results in triangle voids as illustrated in (f). (e) Magnified view in (b) to show triangle voids in h-BN film. The majority of triangle voids can be repaired by dosing additional borazine. However, ∼5% triangular voids cannot be sintered, due to significant lattice mismatch.

islands meet. The merging of three BN islands to form a triangular void is also documented in the magnified STM images in Figure 3 d,e. In most cases, the triangular voids have 60° angles generated by the merging of parallel-aligned triangular islands. However, some of angles are distorted from 60° due to a slight misfit induced by nonparallel alignment of merging triangles. The majority of triangular holes (∼95%) can be filled by increasing the dosage of borazine. However, ∼5% of the holes cannot be annealed regardless of the amount of borazine introduced (Figure 3c), presumably due to the large lattice distortion in the corner of triangle voids where different h-BN islands merge. Incorporation of nitrogen and boron adatoms in the corners and the edges of voids are likely discouraged by the high edge free energy that will be generated consequently.

Fault lines, a type of grain boundary defect, occur wherever misregistry between two growth nuclei prevents their coherent merging at the growth front. On the same terrace, the probability for two distinct fcc domains to merge coherently is low as there are 144 unique adsorption configurations for each nanomesh unit cell, which covers 12 × 12 unit cells of the Ru(0001) surface. Therefore, for substrate with a smaller moiré unit cell, like Pt (9 × 9), the chance for two fcc h-BN domains to merge coherently will be increased to 1/81. Although copper

dx.doi.org/10.1021/ja3117735 | *J. Am. Chem. Soc.* 2013, 135, 2368−2373

is considered as a good lattice-matched substrate with h-BN, it has been reported that different misalignments between h-BN and copper substrate generates 13 different moiré patterns with periodicities ranging from 5 to 14 nm.[36] Hence, the possibility to have the translational misfit when two fcc domains merge on copper is expected to be high. In almost all cases for the growth of h-BN on Ru, distorted BN networks will be formed at the boundaries of fcc−fcc domains with the subsequent generation of tensile strain in the grain boundaries (Figures 4d−f and 5c).

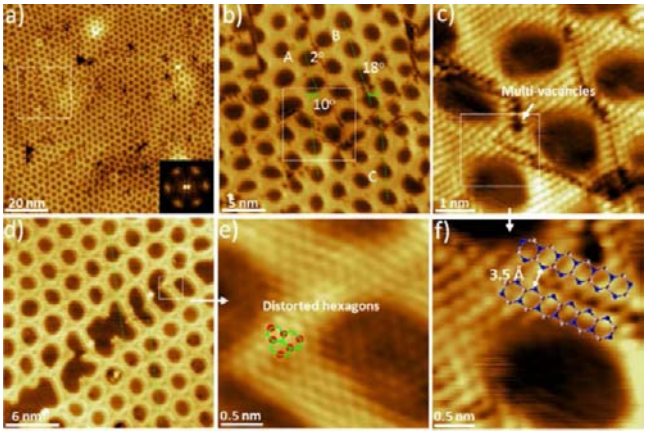

Figure 4. STM images of misfit boundaries in merged h-BN islands. (a) Ru(0001) surface dosed with 30 L borazine at 900 K. (b) Magnified view of the square region in (a) showing fault lines and voids. (c) Fault lines crossing moiré lattice with the detailed atomic structure shown in (d). (e) Distorted h-BN lattice in the boundaries of two fcc h-BN domains merging on the same terrace. (f) Coalescence of 180° misorientated islands terminated by like atoms produces non-bonded interface.

In addition, a non-bonded interface occurs when growth fronts that are terminated by the same atoms, i.e., N atoms, encounter each other. This can happen when the N-terminated edge in island A (fcc domains) encounters the N-terminated edge in island B (hcp domains) (Figure 4c,f, illustrated in Figure 5d). This situation can arise when the thermal barrier between the fcc and hcp domains is overcome by thermal energy (Figure S3).

As mentioned, the smaller energy difference between fcc and hcp domains on Cu or Ni substrate gives rise to a large fraction of coexisting poly domains at higher growth temperature, which will result in a higher density of non-bonded defects when these mismatched domains merge. Since a higher growth temperature is generally needed to allow other forms of defects to be annealed out, the suppression of poly domains by lowering the density of islands, controlled by lowering the growth flux, should be a viable strategy to reduce the density of non-bonded defects in low-pressure CVD growth process. Figure 4f reveals the presence of line defects and multivacancies (<1 nm) in h-BN film caused by the merging of misoriented domains. The majority of these fault lines are due to the misregistry of the h-BN islands because of translational misalignment or twist angles between the domains. For example, as shown in Figure 4d, the two edges along the defective lines are separated by 3.5 Å, which is out of range of N−N or B−N bonding. Figure 4e shows a distorted h-BN lattice at the interface where moiré wires of one domain encounter moiré wires of another domain (Figure 4d). Such distorted boundaries can arise in two situations: sliding misfit in the direction parallel to the edges

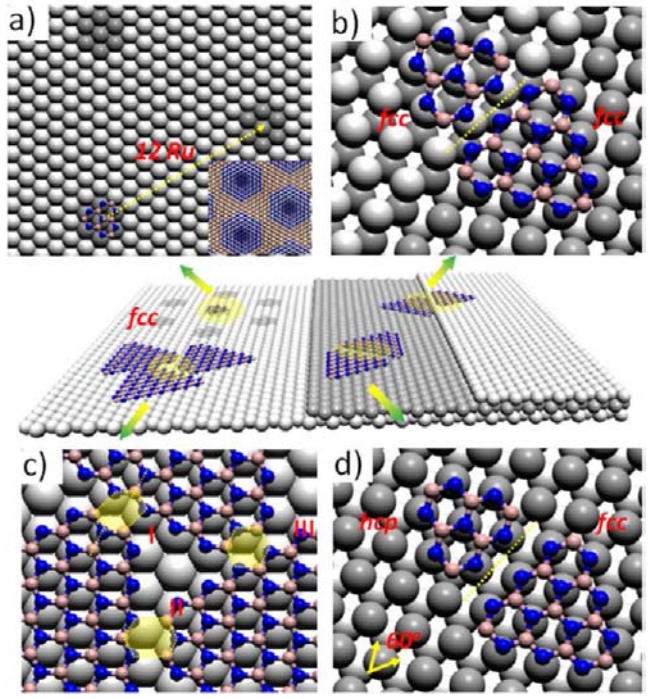

Figure 5. (a) Illustration showing one precise nucleation site out of 144 possibilities for a h-BN island to merge coherently with a second pre-exsiting island. Inset: only when islands nucleate at the center of the moiré pore (dark-blue regions) can they merge coherently. (b) Non-bonded interface is formed between two fcc domains on the adjacent terraces. (c) Distorted h-BN lattice at the interface where different fcc domains merge on the same terrace. I: sliding dislocation induced tilted h-BN lattice; II: strained h-BN lattice due to mismatched space between N-terminated edge and B-terminated tip; and III: h-BN islands merging coherently. (d) Non-bonded interface at the boundary between hcp and fcc domains on the same terrace.

between two fcc domains (I in Figure 5c) or sliding misfit in the direction perpendicular to the edges between the N-terminated edge and B-terminated tip (II in Figure 5c).

Step Flow Growth. Due to the misregistry in individually nucleated BN islands, high-quality h-BN film cannot be grown by the coalescence of discrete h-BN islands. In addition, misfit boundaries will be formed when fcc domains in the upper terrace meet fcc domains on the bottom terrace due to misregistry (N-edge facing N-edge, Figure 5b). This suggests that suppression of nucleation density is needed to improve the film quality. The size of a single crystal h-BN domain will be constrained by the width of the terraces if h-BN film cannot grow over the step edges. One earlier study concluded that h-BN cannot flow continuously across steps on Ru(0001).[26] However, a recent LEEM study reveals that h-BN film shows carpet-like edge flow across substrate edges.[27] Evidence at the atomic level is needed to resolve this issue. Here, we observed that step flow growth is possible as shown in Figure 6a−d when the nucleation density is low. Atomically resolved STM images show that defect-free h-BN lattice covers Ru step edges (Figure 6d,h) continuously. At the step edges, the h-BN moiré pores and wires at the upper and bottom terraces are connected (Figure 6d) seamlessly, which is consistent with the atomic model for the h-BN film aligning with Ru(0001) surface in <11$\bar{2}$0> directions (Figure 6g).

There are two directions (uphill: going up the steps and downhill: going down the steps) for the step flow of h-BN

dx.doi.org/10.1021/ja3117735 | J. Am. Chem. Soc. 2013, 135, 2368−2373

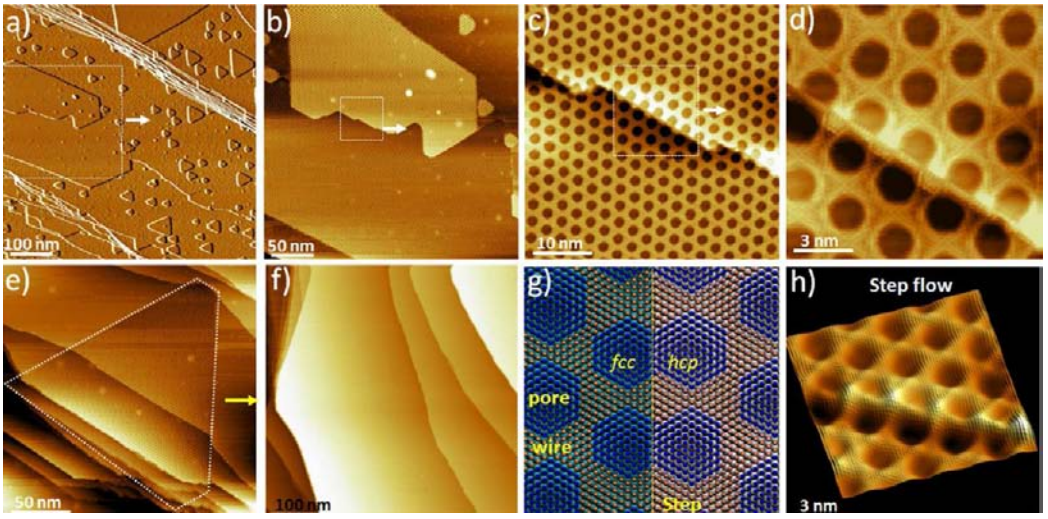

Figure 6. STM images of the growth of h-BN over the step edges of Ru(0001). (a) Derivative STM image to highlight the large-sized single crystal h-BN domain crossing Ru steps. (b) Magnified view of the square region marked in (a). (c) Magnified view of square region marked in (b). (d) STM image of h-BN flowing over step edge. (e) Large-sized single-crystal BN domain grown at 1000 K. (f) A low nucleation density leads to high-quality h-BN film at 1000 K. (g) Atomic structure of h-BN across Ru steps with corresponding alignment of moiré pattern, consistent with that observed in (d). (h) 3-D STM image of h-BN crossing step after FFT filter to visualize the continuity of h-BN film.

across steps. It is believed that step flow in the downhill directions is energetically favorable due to a lower activation energy barrier. However, we have also imaged the step flow of h-BN in the uphill directions (Figure S4). The climb initiates from the moiré wires bridging between the kinks. Hence, the lift-up in the growth front facilitate the step flow in the uphill direction as observed in Figure S4. It is clear that lowering the density of nucleation is crucial for the formation of high-quality h-BN film on Ru(0001). Based on the classical nucleation theory, the density of nuclei should be a function of the ratio between the deposition flux F and the surface diffusion coefficient D. If the deposition rate is slower than diffusion rate, the adsorbed B or N species have sufficient time to diffuse to and enlarge the growing islands instead of forming new nucleation sites. When the individual island expands and meets the step edges, further growth will result in step flow mode. In addition, a high temperature is needed to provide sufficient energy for the small clusters to dissociate and join the large islands by Ostwald ripening process.[37] Therefore, applying a high-temperature growth route to facilitate diffusion while using a low dosage of borazine to suppress nucleation is necessary to promote the step flow mode. A similar strategy had been utilized to sythesize large-area single-crystal graphene by low-pressure CVD.[38,39] This is verified by performing the growth of h-BN at 1100−1200 K with a low partial pressure of borazine at 2×10^{-8} mbar. As shown in Figure 6e, step-flow growth of h-BN across several steps produces single crystal h-BN domain on Ru(0001) (Figure 6f).

CONCLUSION

In summary, the defect formation process during the growth of h-BN monolayer on Ru has been studied systematically from the initial assembly of h-BN triangular clusters to the merging of domains to form mosaic-like films. Our results show that when the nucleation density is high, it is very difficult to form defect-free films because of the intrinsic mismatch between individual h-BN domains on the same terrace as well as between adjacent terraces. Due to the elemental polarity of B and N as well as the large periodicity of the moiré superstructure, the probability for edge-to-edge merging without translational misfit is very low, even when rotational misfit is reduced by the parallel alignment of h-BN triangles on the same terrace. Merging of antiparallel islands across steps or on the same terrace result in a non-bonded fault line, which is a rather unique defect in h-BN when compared to graphene. One strategy to suppress misfit boundaries is to suppress nucleation density during growth, which allows for the step flow growth of h-BN to form large-sized single-crystal domain.

ASSOCIATED CONTENT

Supporting Information

Experimental details and characterization data. This material is available free of charge via the Internet at http://pubs.acs.org.

AUTHOR INFORMATION

Corresponding Author

chmlohkp@nus.edu.sg

Notes

The authors declare no competing financial interest.

ACKNOWLEDGMENTS

This work is supported by MOE Tier 2 project "From in situ observation to the growth scaling of graphene quantum dots (R-143-000-493-112)" and also NRF-CRP project "Novel 2D materials with tailored properties beyond graphene (R-144-000-295-281)".

REFERENCES

(1) Dean, C. R.; Young, A. F.; Meric, I.; Lee, C.; Wang, L.; Sorgenfrei, S.; Watanabe, K.; Taniguchi, T.; Kim, P.; Shepard, K. L.; Hone, J. *Nat. Nanotechnol.* **2010**, *5*, 722−726.

(2) Britnell, L.; Gorbachev, R. V.; Jalil, R.; Belle, B. D.; Schedin, F.; Mishchenko, A.; Georgiou, T.; Katsnelson, M. I.; Eaves, L.; Morozov, S. V.; Peres, N. M. R.; Leist, J.; Geim, A. K.; Novoselov, K. S.; Ponomarenko, L. A. *Science* **2012**, *335*, 947−950.

(3) Britnell, L.; Gorbachev, R. V.; Jalil, R.; Belle, B. D.; Schedin, F.; Katsnelson, M. I.; Eaves, L.; Morozov, S. V.; Mayorov, A. S.; Peres, N.

M. R.; Neto, A. H. C.; Leist, J.; Geim, A. K.; Ponomarenko, L. A.; Novoselov, K. S. *Nano Lett.* **2012**, *12*, 1707−1710.
(4) Liu, Z.; Song, L.; Zhao, S. Z.; Huang, J. Q.; Ma, L. L.; Zhang, J. N.; Lou, J.; Ajayan, P. M. *Nano Lett.* **2011**, *11*, 2032−2037.
(5) Shi, Y. M.; Hamsen, C.; Jia, X. T.; Kim, K. K.; Reina, A.; Hofmann, M.; Hsu, A. L.; Zhang, K.; Li, H. N.; Juang, Z. Y.; Dresselhaus, M. S.; Li, L. J.; Kong, J. *Nano Lett.* **2010**, *10*, 4134−4139.
(6) Kim, K. K.; Hsu, A.; Jia, X. T.; Kim, S. M.; Shi, Y. S.; Hofmann, M.; Nezich, D.; Rodriguez-Nieva, J. F.; Dresselhaus, M.; Palacios, T.; Kong, J. *Nano Lett.* **2012**, *12*, 161−166.
(7) Xue, J. M.; Sanchez-Yamagishi, J.; Bulmash, D.; Jacquod, P.; Deshpande, A.; Watanabe, K.; Taniguchi, T.; Jarillo-Herrero, P.; Leroy, B. J. *Nat. Mater.* **2011**, *10*, 282−285.
(8) Berner, S.; Corso, M.; Widmer, R.; Groening, O.; Laskowski, R.; Blaha, P.; Schwarz, K.; Goriachko, A.; Over, H.; Gsell, S.; Schreck, M.; Sachdev, H.; Greber, T.; Osterwalder, J. *Angew. Chem. Int. Ed.* **2007**, *46*, 5115−5119.
(9) Corso, M.; Auwarter, W.; Muntwiler, M.; Tamai, A.; Greber, T.; Osterwalder, J. *Science* **2004**, *303*, 217−220.
(10) Alem, N.; Yazyev, O. V.; Kisielowski, C.; Denes, P.; Dahmen, U.; Hartel, P.; Haider, M.; Bischoff, M.; Jiang, B.; Louie, S. G.; Zettl, A. *Phys. Rev. Lett.* **2011**, *106*, 126102−126105.
(11) Huang, P. Y.; Ruiz-Vargas, C. S.; van der Zande, A. M.; Whitney, W. S.; Levendorf, M. P.; Kevek, J. W.; Garg, S.; Alden, J. S.; Hustedt, C. J.; Zhu, Y.; Park, J.; McEuen, P. L.; Muller, D. A. *Nature* **2011**, *469*, 389−392.
(12) Liu, Y. Y.; Zou, X. L.; Yakobson, B. I. *ACS Nano* **2012**, *6*, 7053.
(13) Yu, Q. K.; Jauregui, L. A.; Wu, W.; Colby, R.; Tian, J. F.; Su, Z. H.; Cao, H. L.; Liu, Z. H.; Pandey, D.; Wei, D. G.; Chung, T. F.; Peng, P.; Guisinger, N. P.; Stach, E. A.; Bao, J. M.; Pei, S. S.; Chen, Y. P. *Nat. Mater.* **2011**, *10*, 443−449.
(14) Nagashima, A.; Tejima, N.; Gamou, Y.; Kawai, T.; Oshima, C. *Phys. Rev. B* **1995**, *51*, 4606−4613.
(15) Auwarter, W.; Kreutz, T. J.; Greber, T.; Osterwalder, J. *Surf. Sci.* **1999**, *429*, 229−236.
(16) Auwarter, W.; Muntwiler, M.; Osterwalder, J.; Greber, T. *Surf. Sci.* **2003**, *545*, 735−740.
(17) Grad, G. B.; Blaha, P.; Schwarz, K.; Auwarter, W.; Greber, T. *Phys. Rev. B* **2003**, *68*, 085404.
(18) Preobrajenski, A. B.; Vinogradov, A. S.; Martensson, N. *Surf. Sci.* **2005**, *582*, 21−30.
(19) Orlando, F.; Larciprete, R.; Lacovig, P.; Boscarato, I.; Baraldi, A.; Lizzit, S. *J. Phys. Chem. C* **2012**, *116*, 157−164.
(20) Laskowski, R.; Blaha, P. *Phys. Rev. B* **2010**, *81*, 075418−075423.
(21) Cavar, E.; Westerstrom, R.; Mikkelsen, A.; Lundgren, E.; Vinogradov, A. S.; Ng, M. L.; Preobrajenski, A. B.; Zakharov, A. A.; Martensson, N. *Surf. Sci.* **2008**, *602*, 1722−1726.
(22) Preobrajenski, A. B.; Vinogradov, A. S.; Ng, M. L.; Cavar, E.; Westerstrom, R.; Mikkelsen, A.; Lundgren, E.; Martensson, N. *Phys. Rev. B* **2007**, *75*, 245412−245419.
(23) Dong, G. C.; Fourre, E. B.; Tabak, F. C.; Frenken, J. W. M. *Phys. Rev. Lett.* **2010**, *104*, 096102−096105.
(24) Muller, F.; Hufner, S.; Sachdev, H. *Surf. Sci.* **2009**, *603*, 425−432.
(25) Laskowski, R.; Blaha, P.; Gallauner, T.; Schwarz, K. *Phys. Rev. Lett.* **2007**, *98*, 106802−106805.
(26) Goriachko, A.; He, Y. B.; Knapp, M.; Over, H.; Corso, M.; Brugger, T.; Berner, S.; Osterwalder, J.; Greber, T. *Langmuir* **2007**, *23*, 2928−2931.
(27) Sutter, P.; Lahiri, J.; Albrecht, P.; Sutter, E. *ACS Nano* **2011**, *5*, 7303−7309.
(28) Laskowski, R.; Blaha, P.; Schwarz, K. *Phys. Rev. B* **2008**, *78*, 045409−045418.
(29) Soler, J. M.; Artacho, E.; Gale, J. D.; García, A.; Junquera, J.; Ordejón, P.; Sánchez-Portal, D. *J. Phys.: Condens. Matter* **2002**, *14*, 2745−2779.
(30) Troullier, N.; Martins, J. L. *Phys. Rev. B* **1991**, *43*, 1993−2006.
(31) García-Gil, S.; García, A.; Lorente, N.; Ordejón, P. *Phys. Rev. B* **2009**, *79*, 075441−075448.
(32) Lacovig, P.; Pozzo, M.; Alfe, D.; Vilmercati, P.; Baraldi, A.; Lizzit, S. *Phys. Rev. Lett.* **2009**, *103*, 166101−166103.
(33) Cui, Y.; Fu, Q.; Zhang, H.; Bao, X. *Chem. Commun.* **2011**, *47*, 1470−1472.
(34) Wang, B.; Ma, X.; Caffio, M.; Schaub, R.; Li, W. X. *Nano Lett.* **2011**, *11*, 424−430.
(35) Gao, J. F.; Yip, J.; Zhao, J. J.; Yakobson, B. I.; Ding, F. *J. Am. Chem. Soc.* **2012**, *133*, 5009−5015.
(36) Joshi, S.; Ecija, D.; Koitz, R.; Iannuzzi, M.; Seitsonen, A. P.; Hutter, J.; Sachdev, H.; Vijayaraghavan, S.; Bischoff, F.; Seufert, K.; Barth, J. V.; Auwarter, W. *Nano Lett.* **2012**, *12*, 5821−5828.
(37) Lu, J.; Yeo, P. S. E.; Gan, C. K.; Wu, P.; Loh, K. P. *Nat. Nanotech.* **2011**, *6*, 247−252.
(38) Li, X. S.; Magnuson, C. W.; Venugopal, A.; An, J. H.; Suk, J. W.; Han, B. Y.; Borysiak, M.; Cai, W. W.; Velamakanni, A.; Zhu, Y. W.; Fu, L. F.; Vogel, E. M.; Voelkl, E.; Colombo, L.; Ruoff, R. S. *Nano Lett.* **2010**, *10*, 4328−4334.
(39) Li, X. S.; Magnuson, C. W.; Venugopal, A.; Tromp, R. M.; Hannon, J. B.; Vogel, E. M.; Colombo, L.; Ruoff, R. S. *J. Am. Chem. Soc.* **2011**, *133*, 2816−2819.